NANO LETTERS

pubs.acs.org/NanoLett
Letter

Engineering Two-Dimensional Nodal Semimetals in Functionalized Biphenylene by Fluorine Adatoms

Seongjun Mo, Jaeuk Seo, Seok-Kyun Son, Sejoong Kim,* Jun-Won Rhim,* and Hoonkyung Lee*

Cite This: *Nano Lett.* 2024, 24, 4885−4892

ABSTRACT: We propose a band engineering scheme on the biphenylene network, a newly synthesized carbon allotrope. We illustrate that the electronic structure of the biphenylene network can be significantly altered by controlling conditions affecting the symmetry and destructive interference of wave functions through periodic fluorination. First, we investigate the mechanism for the appearance of a type-II Dirac fermion in a pristine biphenylene network. We show that the essential ingredients are mirror symmetries and stabilization of the compact localized eigenstates via destructive interference. While the former is used for the band-crossing point along high symmetry lines, the latter induces highly inclined Dirac dispersions. Subsequently, we demonstrate the transformation of the biphenylene network's type-II Dirac semimetal phase into various Dirac phases such as type-I Dirac, gapped type-II Dirac, and nodal line semimetals through the deliberate disruption of mirror symmetry or modulation of destructive interference by varying the concentration of fluorine atoms.

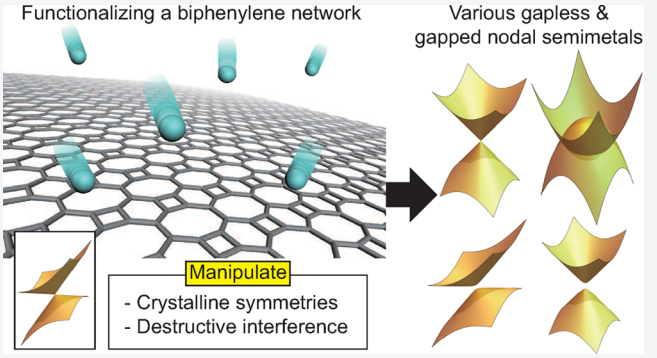

KEYWORDS: *biphenylene, flat band, Dirac semimetal, fluorination*

Triggered by the discovery of carbon nanotubes,[1,2] studies on low dimensional carbon allotropes, such as graphene, have significantly proliferated because one can have a variety of intriguing electronic structures depending on the arrangement of carbon atoms. For example, one can have massless Dirac fermions in graphene,[3,4] whereas infinitely heavy particles can also appear in another honeycomb network of carbon atoms called the cyclic-graphdiyne, which hosts a singular flat band.[5,6] In the case of graphene, relying on its high structural stability, one can further engineer the band structure to obtain flat bands by tailoring it into ribbon geometries[7] or twisting two stacked graphene sheets.[8,9] These peculiar electronic structures have received great attention because they are relevant to the possible many-body phases such as ferromagnetism[10,11] and superconductivity.[12−15]

Recently, another type of two-dimensional carbon allotrope, called the biphenylene network (BPN), was synthesized[16] and has attracted significant interests in various properties of BPN layers including electronic, optical, mechanical, thermal, magnetic, and chemical properties.[17−53] Moreover, from the first-principles analysis, BPN turned out to exhibit another intriguing band dispersion called type-II Dirac fermion consisting of two heavily inclined cones, so that we have open Fermi surfaces instead of Fermi points or circles.[17,18] In type-II Dirac semimetals,[54] one can have electron- and hole-type carriers simultaneously in contrast to the type-I case such as graphene. This intricate band shape may lead to a variety of unusual electronic phenomena such as anisotropic transport and magnetoresistance behavior[55−58] and undamped gapless plasmon modes.[59] Therefore, engineering their band shapes is important to tune their electronic properties for applications.

In this Letter, we first analyze the origin of the type-II Dirac dispersion of the pristine BPN from the perspective of destructive interference and symmetry. The essential feature of the type-II Dirac dispersion of the pristine BPN is that it is inclined so that a flat band with a zero Fermi velocity appears along a high symmetry line, while the Dirac band-crossing is protected by mirror symmetry. We show that the pristine BPN hosts a proper destructive interference stabilizing a stripe-type compact localized state, which signals the existence of a flat band, along the mirror-symmetric axis in momentum space. This implies that one can engineer the electronic structures of the BPN by controlling the conditions for destructive interference and symmetries. We demonstrate that this can be done successfully by absorbing fluorine atoms at various positions. We show that we can have diverse Dirac dispersions of different kinds, such as type-I, massive, and nodal line Dirac fermions, by fluorinating the BPN periodically.

Received: January 20, 2024
Revised: April 10, 2024
Accepted: April 10, 2024
Published: April 12, 2024

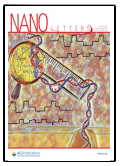

https://doi.org/10.1021/acs.nanolett.4c00314
Nano Lett. 2024, 24, 4885−4892

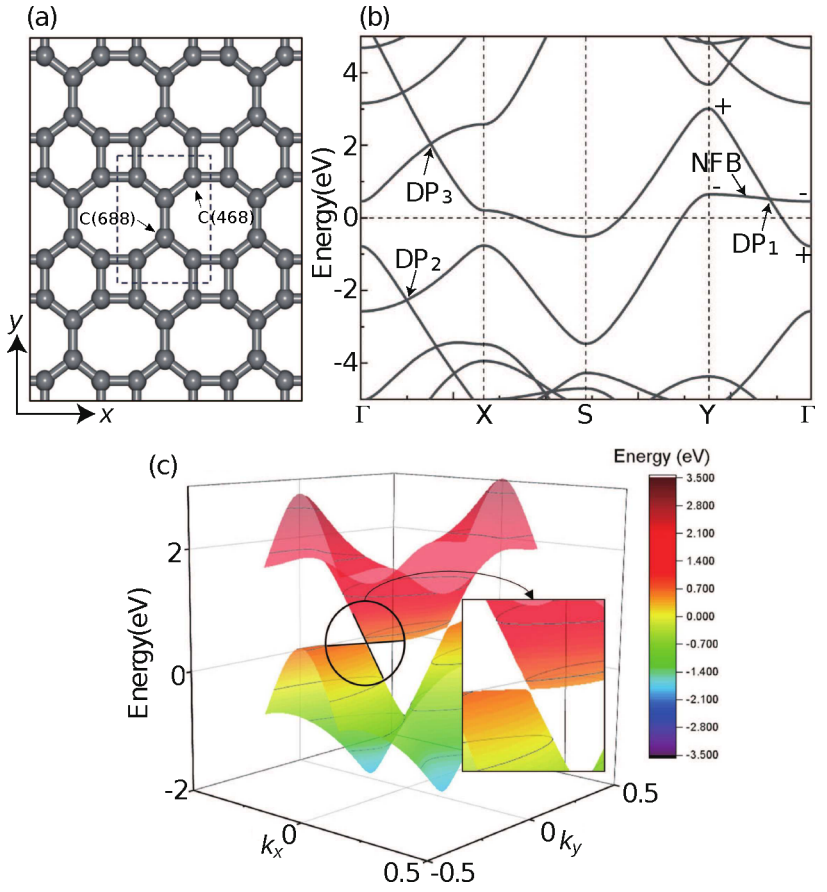

Figure 1. (a) The lattice structure, (b) band structure, and (c) 3D energy structure near the ΓY line of pristine BPN. The unit cell is represented by a dashed box in (a). Several Dirac points are denoted by DP_1, DP_2, and DP_3 in (b). NFB indicates the nearly flat band.

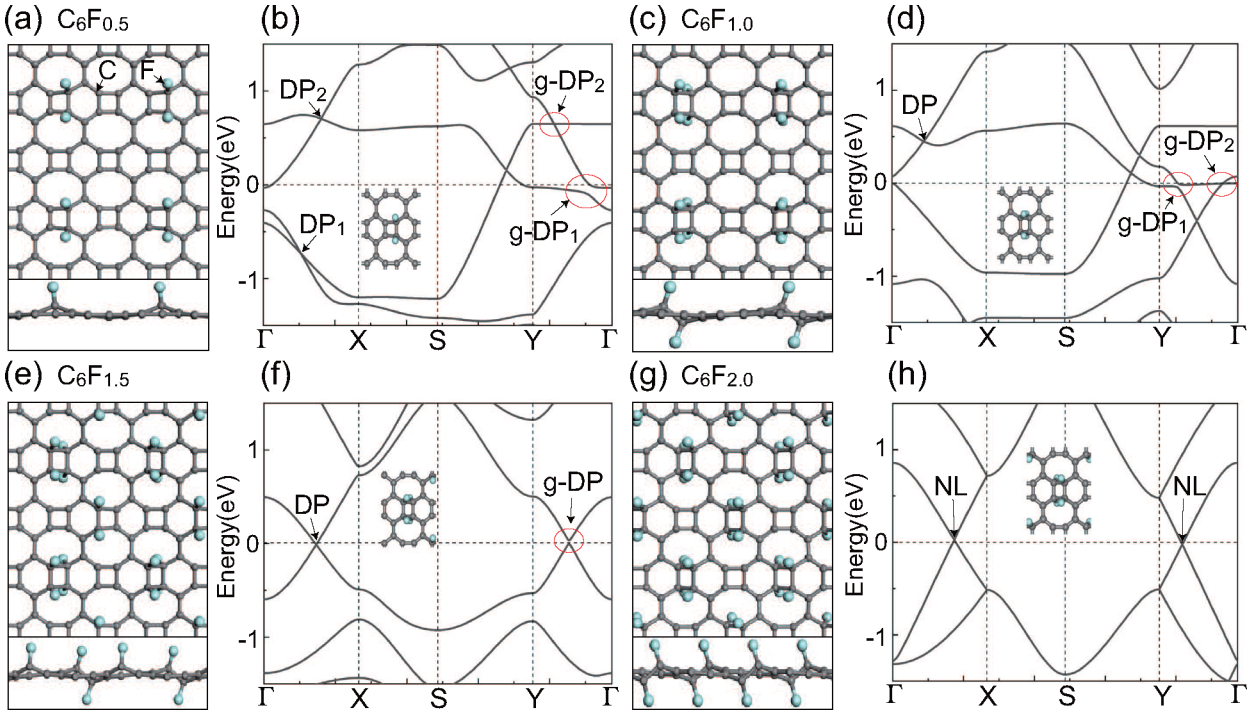

Figure 2. Optimized geometries of fluorinated BPN monolayers with different concentrations of fluorine and their electronic structures: (a, b) $C_6F_{0.5}$, (c, d) $C_6F_{1.0}$, (e, f) $C_6F_{1.5}$, and (g, h) $C_6F_{2.0}$. Gray (cyan) spheres represent carbon (fluorine) atoms. Dirac nodes, gapped-Dirac points, and nodal lines are denoted by DP, g-DP, and NL, respectively.

https://doi.org/10.1021/acs.nanolett.4c00314
Nano Lett. 2024, 24, 4885−4892

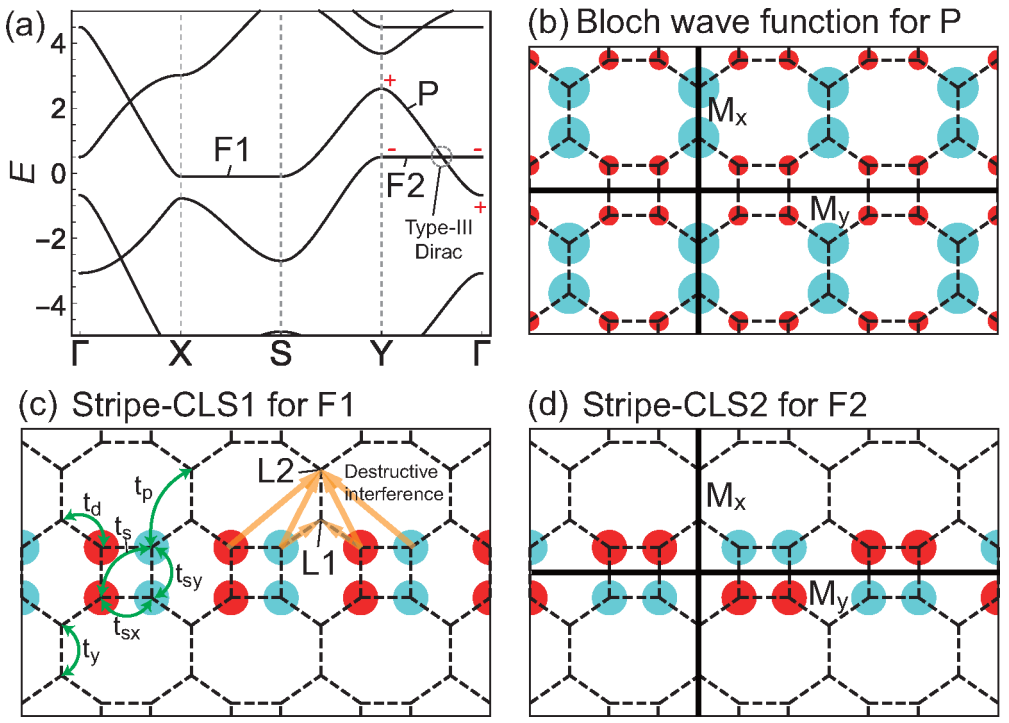

Figure 3. (a) The tight-binding band structures of the pristine BPN with band parameters $\{t_{sx}, t_{sy}, t_y, t_d, t_s, t_p, E_0\} = \{-3, -2.7, -2.7, -2.8, -0.7, 0, -0.5\}$. We indicate the 1D flat bands along XS and YΓ by F1 and F2, respectively. The parabolic band crossing with the flat band F2 is denoted by P. (b) Bloch wave function corresponding to the parabolic band P at Γ. Colored circles represent the amplitudes of the wave function. Red (cyan) color implies that the sign of the amplitude is 1 (−1), while the radius of the circle is proportional to the magnitude of the amplitude. Thick vertical and horizontal lines represent the mirror symmetry planes. In (c) and (d), we illustrate the stripe-CLS1 and stripe-CLS2 corresponding to the flat bands F1 and F2, respectively. In (c), the hopping processes are summarized. The CLS can be an eigenmode even if the longer-ranged hopping processes represented by the yellow arrow are further included due to the destructive interference at sites L1 and L2.

To investigate the geometrical and electronic properties of pristine single-layer BPN, we perform geometry optimization of BPN using first-principles calculations based on density functional theory (DFT). The optimized geometry and energy bands of BPN are shown in Figure 1(a) and (b), respectively. As in the previous study,[17,18] we observe a couple of type-II Dirac points whose Dirac nodes lie on ΓY near the Fermi energy E_F as denoted by DP_1 in Figure 1(b). As highlighted in Figure 1(c), there are two tilted Dirac dispersions around the Γ point. corresponding to DP_1 in Figure 1(b). While the Dirac point is developed by the crossing of two bands along ΓY, it is essential that one of them is almost flat for realizing a type-II Dirac fermion. Therefore, it is crucial to understand the origin of the flat dispersion along ΓY to reveal the mechanism for the appearance of the type-II Dirac semimetal, which will be discussed in the following subsection.

We introduce fluorine atoms to a single-layer BPN to engineer its electronic structures. A single-layer BPN has two distinct carbon sites that fluorine atoms can attach to in a primitive cell: one located at the junction of one hexagon and two octagons and the other located at the junction of one square, one hexagon, and one octagon. We denote the first site and the second one by C(688) and C(468), respectively, as shown in Figure 1(a). Regarding a pristine BPN monolayer, binding energies of fluorine (F) atoms to carbon sites are computed as follows: 3.20 eV/F for C(468) and 2.21 eV/F for C(688). It implies that F atoms energetically prefer to bind to C(468) rather than C(688). Varying fluorine concentrations x, we consider four fluorinated BPN layers C_6F_x for x = 0.5, 1.0, 1.5, and 2.0, whose atomic structures are displayed in Figures 2(a), (c), (e), and (g), respectively. DFT calculations also reveal that F atoms energetically prefer to attach to the C(468) sites for higher F concentrations. Corresponding binding energies of F to C(468) sites are 3.45, 3.51, 3.48, and 3.50 eV/F for x = 0.5, 1.0, 1.5, and 2.0, respectively. All structures of the four fluorinated BPN layers are fully relaxed, and their dynamic stability is verified by calculating phonon dispersions as shown in Supporting Figure 6.[60,61]

Band structures of the fluorinated BPNs are plotted on the right side of the atomic configurations in Figure 2. Intriguingly, diverse nodal states emerge depending on the F concentrations. At fluorine concentrations of 0.5 and 1.0, gapped type-II Weyl nodes are found as a result of crossing between flat bands near E_F along ΓY and energy bands hosting saddle-point van Hove singularity (vHS) at Y. See the red circles in Figure 2(b) and (d). This gap opening is attributed to the mirror symmetry breaking with respect to the monolayer BPN plane due to fluorine attachment. On the other hand, we found gapless and gapped type-I Dirac points along the x- and y-axis in $C_6F_{1.5}$ as shown in Figure 2(f) while nodal rings appear in C_6F_2 as noted in Figure 2(h). For clarity, we provide 3D band structures of these two compounds in Supporting Figure 3. An effective Hamiltonian is formulated using a tight-binding model in the next subsection to provide a more accurate interpretation.

To understand how the variety of relativistic dispersions can be stabilized in pristine BPN and fluorinated BPNs, we conduct an analysis of their wave function symmetries. Here, we first focus on the protection or gap-opening mechanisms of the nodal points or lines, while the origin of the inclination in

https://doi.org/10.1021/acs.nanolett.4c00314
Nano Lett. 2024, 24, 4885−4892

Dirac dispersions is addressed in the next subsection. Specifically, we consider only the wave functions of the bands near the Fermi level. The symmetries of the wave functions are visualized by plotting the amplitudes of the Bloch wave function at the Γ point as illustrated in Supporting Figure 2. For the pristine BPN, one can show that the band-crossing along ΓY in Figure 1(b) is protected by the mirror symmetry with respect to the yz plane, which is denoted by M_x. The nearly flat band (NFB) and the dispersive band, which constitute the type-II Dirac point, correspond to the mirror eigenvalues −1 and 1, respectively, as shown in Supporting Figure 2(a). Furthermore, upon close inspection of the wave function depicted in Supporting Figure 2(a), an intriguing resemblance to the anti-bond wave function of benzene becomes apparent. This finding may imply a potential connection between the electronic properties of the material under investigation and those of benzene, which is known for its aromatic properties and unique bonding characteristics.

On the other hand, the mirror symmetry M_x is broken in $C_6F_{0.5}$ and C_6F_1. As a result, the wave functions are not mirror-symmetric with respect to the yz plane as shown in Supporting Figure 2(b) and (c), and band crossings along ΓY are all gapped out, realizing massive type-II Dirac fermions as shown in Figure 2(b) and (d). Although several type-II Dirac nodes, denoted by g-DP_2 in Figure 2(b) and (d), look gapless, they actually have tiny gaps whose energy is about 0.1 meV. Note that $C_6F_{0.5}$ and C_6F_1 respect the mirror symmetry M_y with respect to the zx plane, so their wave functions are either mirror symmetric or mirror anti-symmetric as illustrated in Supporting Figure 2(b) and (c). Thus, band-crossings indicated by DP_1 and DP_2 in Figure 2(b) and DP in Figure 2(d) are protected along ΓX. As like the two previous compounds, $C_6F_{1.5}$ satisfies only the mirror symmetry M_y, so it has gapless and gapped-out Dirac nodes on ΓX and ΓY, respectively. See Figure 2(f). In contrast to $C_6F_{0.5}$ and C_6F_1, $C_6F_{1.5}$ does not stabilize flat bands, resulting exclusively in type-I Dirac fermions. Finally, in C_6F_2, both mirror symmetries M_x and M_y are respected. The system, therefore, becomes gapless along both ΓX and ΓY as illustrated in Figure 2(h). In fact, these two nodes are part of the nodal line.

In this subsection, we discuss another crucial condition for the appearance of type-II Dirac fermions in pristine BPN and the aforementioned fluorinated BPNs by analyzing how flat bands are stabilized along certain symmetry axes. To this end, we apply a tight-binding method, which is advantageous for flat band analysis. The essential mechanism for the development of the dispersionless band is the existence of a compact localized state (CLS), which is a localized eigenstate having nonzero amplitudes only inside a finite region.[62−65] Although electrons can move on the lattice via hopping processes, such an extremely localized mode can exist due to the destructive interference hosted by the special lattice structures. The CLS is considered a characteristic eigenstate of a flat band because it is guaranteed to exist when it is completely flat.[64] While one can have N (the number of unit cells) for different CLSs centered at different positions, they are not independent of each other if the Bloch eigenstate corresponding to the flat band possesses a discontinuity in momentum space. Such a flat band is called a singular flat band, and its geometric and topological aspects have been studied extensively.[6,64−67]

First, regarding the fact that energy bands of our interest mostly originate from p_z orbitals of carbon atoms, we construct an effective tight-binding model consisting of the six p_z orbitals for the pristine BPN to understand the origin of its flat bands along ΓY and XS, as shown in Figure 3(a). Along these lines, the Hamiltonian can be regarded effectively as a one-dimensional system hosting flat bands. The effective 1D Hamiltonians along ΓY and XS are obtained by the inverse Fourier transform of the Bloch Hamiltonian with $k_x = 0$ and $k_x = \pi$, respectively. Therefore, we seek a CLS compactly localized along the y-axis in order to understand the origin of flat bands. Six tight-binding parameters are denoted by t_{sx}, t_{sy}, t_y, t_d, t_s, and t_p as represented in Figure 3(c). Main features of the DFT calculations can be captured by the tight-binding parameters $\{t_{sx}, t_{sy}, t_y, t_d, t_s, t_p, E_0\} = \{-3, -2.7, -2.7, -2.8, -0.7, -0.3, -0.5\}$, where E_0 is the overall energy shift. Two perfectly flat bands around the Fermi level along ΓY and XS are denoted by F1 and F2, respectively. Their energies are given by $E_{F1} = -t_p - t_s + t_{sx} - t_{sy} + E_0$ and $E_{F2} = -t_p - t_s - t_{sx} + t_{sy} + E_0$. The flatness of these flat bands is robust against variation of those tight-binding parameters. The CLSs corresponding to the flat bands F1 and F2 are plotted in Figure 3(c) and (d). As the effective Hamiltonians are translationally invariant along the y-axis, the CLSs are compactly localized along the same direction. On the other hand, they are extended along the x-direction modulating with the fixed momenta $k_x = 0$ and $k_x = \pi$. These CLSs are denoted as the stripe-CLSs. One can notice that the lattice structure provides a destructive interference at the sites linking two neighboring square plaquettes of carbon atoms, denoted by L_1, as explained in Figure 3(c). While the flat band F2 has a Dirac band-crossing with a dispersive band, this is protected by mirror symmetry M_x because the CLS and the wave functions in the dispersive band have mirror eigenvalues −1 and +1, respectively, as shown in Figure 3(b) and (d). This band-crossing between the flat and dispersive bands results in a type-II Dirac fermion, as plotted in Figure 3(a). Note that a long-range hopping t_p does not break the flatness of the flat band because this hopping process also offers destructive interference for the same CLS, denoted by L_2 in Figure 3(c). In fact, what we have obtained so far belongs to the type-III Dirac fermion because the dispersion is perfectly flat along a direction.[68] Depending on the values of longer-range hopping parameters, this type-III Dirac semimetal transforms into type-I or type-II Dirac fermions, as shown in DFT calculations. Although the longer-range hybridizations would not provide such a destructive interference and, therefore, deform the flat band, the resultant bandwidth is tiny, as we observed in DFT calculations because their hopping amplitudes should be much smaller than the nearest neighbor ones. Even if the flat band is warped, the band-crossing is robust against the inclusion of the long-range processes, because mirror symmetry is still respected. The pristine BPN has another mirror symmetry M_y, and the type-I Dirac dispersions along ΓX are protected by it.

As a next step, we show that by fluorinating BPN, such as $C_6F_{0.5}$ and C_6F_1, we can have gapped type-II Weyl semimetals. In the tight-binding analysis, the fluorination is assumed to be equivalent to making a vacancy at the corresponding carbon site. This assumption is reasonable since hybridization between the p_z orbital and fluorine atoms leads to bonding and anti-bonding states whose energies might be pushed away from the energy window of our interest. For $C_6F_{0.5}$ and C_6F_1, stripe-CLSs can still be stabilized along the chain of square plaquettes of carbon atoms, which are not fluorinated and extended along the x-axis, as shown in Figure 4(a) and (b). As a result, the flat

https://doi.org/10.1021/acs.nanolett.4c00314
Nano Lett. 2024, 24, 4885−4892

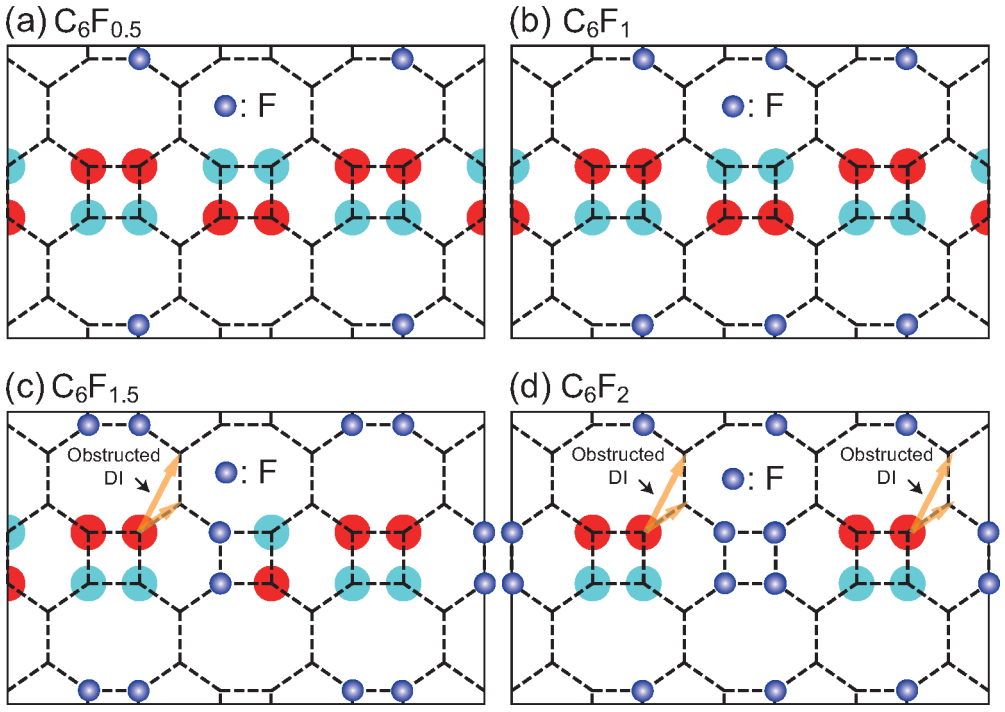

Figure 4. In (a) and (b), the stripe-CLSs of $C_6F_{0.5}$ and C_6F_1 are plotted. They occupy the chain of square plaquettes of carbon atoms in the middle. The attached fluorine atoms are represented by blue circles. The red and cyan circles indicate plus and minus signs, respectively. In (c) and (d), we show that the stabilization of the stripe-CLSs fails due to the obstructed destructive interference (DI) by fluorine atoms in the middle chain of the square plaquettes.

bands appear along ΓY and XS, as shown by the nearly flat bands in the DFT band structures in Figure 2(b) and (d). However, due to the broken mirror symmetry by the fluorine atoms, any band-crossing along these high-symmetry lines does not have to be protected. Indeed, all of the band-crossings of type-II Dirac dispersions along ΓY are gapped out, as discussed in the previous subsection. In the case of $C_6F_{0.5}$, we note that the energy gap at the higher Dirac point (g-DP_2) is tiny but nonzero. Namely, we obtained massive type-II Dirac fermions by fluorination, which breaks mirror symmetry while maintaining destructive interference. Since the attached fluorine atoms do not break M_y, type-I Dirac dispersions along ΓX and SY are all immune from being gapped out. If we attach more fluorine atoms, any stripe-CLSs cannot be an eigenmode because all of the possible destructive interferences are obstructed by the fluorine atoms, as shown in Figure 4(c) and (d). Therefore, we cannot expect flat bands in $C_6F_{1.5}$ and C_6F_2, and no type-II Dirac semimetals are expected in these compounds. Instead, type-I and nodal line semimetals appear, as shown in the DFT calculations.

In this paper, we have shown that a variety of Dirac particles, such as massless or massive type-I and -II Dirac, and a nodal line can be obtained by the manipulated fluorination on the BPN. In our band engineering scheme, it is crucial that one can eliminate destructive interference and mirror symmetries by properly locating the fluorine atoms. Especially the concept of controlling destructive interference is first proposed in this paper, showing that one can manipulate the electronic structure of a solid by reshaping its wave function in real space. While we have focused on a specific material system, our work eventually proposes a novel band engineering method, where we control the slope of a part of the Dirac dispersion by manipulating the condition for destructive interference via the molecular absorption technique.

Attaching atoms to two-dimensional lattices or surfaces on a microscopic level is experimentally feasible. By using scanning tunneling microscopy (STM), hydrogen atoms or CO molecules can be absorbed and controlled on a graphene or Cu(111) surface on the atomic scale,[69,70] and even an automated manipulation of their position is possible.[71] Moreover, the fluorination of another carbon allotrope, graphene, has been extensively studied.[72−76] Therefore, we believe that our band engineering scheme can be realized in experiments so that fluorinated BPN could be an ideal platform to study intriguing phenomena from various types of Dirac dispersions and flat bands.

■ ASSOCIATED CONTENT

Supporting Information

The Supporting Information is available free of charge at https://pubs.acs.org/doi/10.1021/acs.nanolett.4c00314.

Computational details for the DFT simulations, symmetry analysis of Bloch wave functions, 3D band disperions of $C_6F_{1.5}$ and $C_6F_{2.0}$, and band dispersions of $C_6Cl_{0.5}$ and $C_6Br_{0.5}$ (PDF)

■ AUTHOR INFORMATION

Corresponding Authors

Hoonkyung Lee − *Department of Physics, Konkuk University, Seoul 05029, Korea; Research Center for Novel Epitaxial Quantum Architectures, Department of Physics, Seoul National University, Seoul 08826, Korea;* orcid.org/0000-0002-6417-1648; Email: hkiee3@konkuk.ac.kr

Jun-Won Rhim − *Research Center for Novel Epitaxial Quantum Architectures, Department of Physics, Seoul*

https://doi.org/10.1021/acs.nanolett.4c00314
Nano Lett. 2024, 24, 4885−4892

National University, Seoul 08826, Korea; Department of Physics, Ajou University, Suwon 16499, Korea; orcid.org/0000-0001-9094-0650; Email: jwrhim@ajou.ac.kr

Sejoong Kim − *University of Science and Technology (UST), Daejeon 34113, Korea; Korea Institute for Advanced Study, Seoul 02455, Korea;* orcid.org/0000-0002-9140-7353; Email: sejoong@alum.mit.edu

Authors

Seongjun Mo − *Department of Physics, Konkuk University, Seoul 05029, Korea*

Jaeuk Seo − *Department of Physics, Ajou University, Suwon 16499, Korea; Department of Physics, Korea Advanced Institute of Science and Technology, Daejeon 34141, Korea*

Seok-Kyun Son − *Department of Physics and Department of Information Display, Kyung Hee University, Seoul 02447, Republic of Korea*

Complete contact information is available at: https://pubs.acs.org/10.1021/acs.nanolett.4c00314

Author Contributions

S.M. and J.S. contributed equally. S.M. conducted the DFT analysis. J.S. conducted the tight-binding analysis. H.L., J.-W.R., S.K., and S.-K.S. conducted the results discussion. H.L., J.-W.R., and S.K. supervised the study and wrote, reviewed, and revised the manuscript.

Notes

The authors declare no competing financial interest.

■ ACKNOWLEDGMENTS

H.L. and J.-W.R. are supported by the National Research Foundation of Korea (NRF) Grant funded by the Korean government (MSIT) (Grant No. 2021R1A5A1032996). J.-W.R. is supported by the National Research Foundation of Korea (NRF) Grant funded by the Korean government (MSIT) (Grant Nos. 2021R1A2C1010572 and 2022M3H3-A106307411) and the Ministry of Education (Grant No. RS-2023-00285390). S.K. is supported by the National Research Foundation of Korea (NRF) grant funded by the Korea government (Grant No. NRF-2022R1F1A1074670). S.-K.S. acknowledges the support by the National Research Foundation of Korea (NRF) grant funded by the Korea government (MSIT) (2022R1A5A8033794).

■ REFERENCES

(1) Iijima, S. Helical microtubules of graphitic carbon. *Nature* **1991**, *354*, 56.

(2) Dresselhaus, M.; Dresselhaus, G.; Saito, R. Physics of carbon nanotubes. *Carbon* **1995**, *33*, 883.

(3) Novoselov, K. S.; Geim, A. K.; Morozov, S. V.; Jiang, D.-e.; Zhang, Y.; Dubonos, S. V.; Grigorieva, I. V.; Firsov, A. A. Electric field effect in atomically thin carbon films. *science* **2004**, *306*, 666.

(4) Zhang, Y.; Tan, Y.-W.; Stormer, H. L.; Kim, P. Experimental observation of the quantum hall effect and berry's phase in graphene. *nature* **2005**, *438*, 201.

(5) You, J.-Y.; Gu, B.; Su, G. Flat band and hole-induced ferromagnetism in a novel carbon monolayer. *Sci. Rep.* **2019**, *9*, 20116.

(6) Rhim, J.-W.; Kim, K.; Yang, B.-J. Quantum distance and anomalous landau levels of flat bands. *Nature* **2020**, *584*, 59.

(7) Son, Y.-W.; Cohen, M. L.; Louie, S. G. Energy gaps in graphene nanoribbons. *Phys. Rev. Lett.* **2006**, *97*, 216803.

(8) Cao, Y.; Fatemi, V.; Fang, S.; Watanabe, K.; Taniguchi, T.; Kaxiras, E.; Jarillo-Herrero, P. Unconventional superconductivity in magic-angle graphene superlattices. *Nature* **2018**, *556*, 43.

(9) Tarnopolsky, G.; Kruchkov, A. J.; Vishwanath, A. Origin of magic angles in twisted bilayer graphene. *Phys. Rev. Lett.* **2019**, *122*, 106405.

(10) Mielke, A. Ferromagnetism in the hubbard model and hund's rule. *Phys. Lett. A* **1993**, *174*, 443.

(11) Tasaki, H. From nagaoka's ferromagnetism to flat-band ferromagnetism and beyond: an introduction to ferromagnetism in the hubbard model. *Progress of theoretical physics* **1998**, *99*, 489.

(12) Volovik, G. The fermi condensate near the saddle point and in the vortex core. *JETP Letters* **1994**, *59*, 830.

(13) Balents, L.; Dean, C. R.; Efetov, D. K.; Young, A. F. Superconductivity and strong correlations in moiré flat bands. *Nat. Phys.* **2020**, *16*, 725.

(14) Peri, V.; Song, Z.-D.; Bernevig, B. A.; Huber, S. D. Fragile topology and flat-band superconductivity in the strong-coupling regime. *Physical review letters* **2021**, *126*, 027002.

(15) Volovik, G. E. Graphite, graphene, and the flat band superconductivity. *JETP Letters* **2018**, *107*, 516.

(16) Fan, Q.; Yan, L.; Tripp, M. W.; Krejčí, O.; Dimosthenous, S.; Kachel, S. R.; Chen, M.; Foster, A. S.; Koert, U.; Liljeroth, P.; Gottfried, J. M. Biphenylene network: A nonbenzenoid carbon allotrope. *Science* **2021**, *372*, 852.

(17) Son, Y.-W.; Jin, H.; Kim, S. Magnetic ordering, anomalous Lifshitz transition, and topological grain boundaries in two-dimensional biphenylene network. *Nano Lett.* **2022**, *22*, 3112.

(18) Liu, P.-F.; Li, J.; Zhang, C.; Tu, X.-H.; Zhang, J.; Zhang, P.; Wang, B.-T.; Singh, D. J. Type-II Dirac cones and electron-phonon interaction in monolayer biphenylene from first-principles calculations. *Phys. Rev. B* **2021**, *104*, 235422.

(19) Demirci, S.; Çallıoğlu, i. m. c.; Görkan, T.; Aktürk, E.; Ciraci, S. Stability and electronic properties of monolayer and multilayer structures of group-IV elements and compounds of complementary groups in biphenylene network. *Phys. Rev. B* **2022**, *105*, 035408.

(20) Luo, Y.; Ren, C.; Xu, Y.; Yu, J.; Wang, S.; Sun, M. A first principles investigation on the structural, mechanical, electronic, and catalytic properties of biphenylene. *Sci. Rep.* **2021**, *11*, 19008.

(21) Rublev, P.; Tkachenko, N. V.; Boldyrev, A. I. Overlapping electron density and the global delocalization of π-aromatic fragments as the reason of conductivity of the biphenylene network. *J. Comput. Chem.* **2023**, *44*, 168.

(22) Liu, G.; Chen, T.; Li, X.; Xu, Z.; Xiao, X. Electronic transport in biphenylene network monolayer: Proposals for 2D multifunctional carbon-based nanodevices. *Appl. Surf. Sci.* **2022**, *599*, 153993.

(23) Chowdhury, S.; Ghosal, S.; Mondal, D.; Jana, D. First-principles and machine-learning study of electronic and phonon transport in carbon-based AA-stacked bilayer biphenylene nanosheets. *J. Phys. Chem. Solids* **2022**, *170*, 110909.

(24) Shen, H.; Yang, R.; Xie, K.; Yu, Z.; Zheng, Y.; Zhang, R.; Chen, L.; Wu, B.-R.; Su, W.-S.; Wang, S. Electronic and optical properties of hydrogen-terminated biphenylene nanoribbons: a first-principles study. *Phys. Chem. Chem. Phys.* **2021**, *24*, 357.

(25) Xie, Y.; Chen, L.; Xu, J.; Liu, W. Effective regulation of the electronic properties of a biphenylene network by hydrogenation and halogenation. *RSC Adv.* **2022**, *12*, 20088.

(26) Wang, K.; Ren, K.; Zhang, D.; Cheng, Y.; Zhang, G. Phonon properties of biphenylene monolayer by first-principles calculations. *Appl. Phys. Lett.* **2022**, *121*, 042203.

(27) Hamed Mashhadzadeh, A.; Zarghami Dehaghani, M.; Molaie, F.; Fooladapanjeh, S.; Farzadian, O.; Spitas, C. A theoretical insight into the mechanical properties and phonon thermal conductivity of biphenylene network structure. *Comput. Mater. Sci.* **2022**, *214*, 111761.

(28) Mortazavi, B.; Shapeev, A. V. Anisotropic mechanical response, high negative thermal expansion, and outstanding dynamical stability of biphenylene monolayer revealed by machine-learning interatomic potentials. *FlatChem.* **2022**, *32*, 100347.

(29) Pereira, M. L.; da Cunha, W. F.; de Sousa, R. T.; Amvame Nze, G. D.; Galvão, D. S.; Ribeiro, L. A. On the mechanical properties and fracture patterns of the nonbenzenoid carbon allotrope (biphenylene

network): a reactive molecular dynamics study. *Nanoscale* **2022**, *14*, 3200.
(30) Ren, X.; Wang, K.; Yu, Y.; Zhang, D.; Zhang, G.; Cheng, Y. Tuning the mechanical anisotropy of biphenylene by boron and nitrogen doping. *Comput. Mater. Sci.* **2023**, *222*, 112119.
(31) Bafekry, A.; Faraji, M.; Fadlallah, M. M.; Jappor, H. R.; Karbasizadeh, S.; Ghergherehchi, M.; Gogova, D. Biphenylene monolayer as a two-dimensional nonbenzenoid carbon allotrope: a first-principles study. *J. Phys.: Condens. Matter* **2022**, *34*, 015001.
(32) Yang, N.; Chen, Q.; Xu, Y.; Luo, J.; Yang, H.; Jin, G. Strain-modulated electronic transport in two-dimensional carbon allotropes. *AIP Advances* **2022**, *12*, 045102.
(33) Zhang, L.; Tong, P. Even-odd chain dependent spin valve effect on a zigzag biphenylene nanoribbon junction. *J. Phys.: Condens. Matter* **2022**, *34*, 395301.
(34) Alcón, I.; Calogero, G.; Papior, N.; Antidormi, A.; Song, K.; Cummings, A. W.; Brandbyge, M.; Roche, S. Unveiling the multiradical character of the biphenylene network and its anisotropic charge transport. *Journal of the American Chemical* **2022**, *144*, 8278.
(35) Ren, K.; Shu, H.; Huo, W.; Cui, Z.; Xu, Y. Tuning electronic, magnetic and catalytic behaviors of biphenylene network by atomic doping. *Nanotechnology* **2022**, *33*, 345701.
(36) Ge, Y.; Wang, Z.; Wang, X.; Wan, W.; Liu, Y. Superconductivity in the two-dimensional nonbenzenoid biphenylene sheet with Dirac cone. *2D Materials* **2022**, *9*, 015035.
(37) Liu, G.-H.; Yang, L.; Qiao, S.-X.; Jiao, N.; Chen, Y.-J.; Ni, M.-Y.; Zheng, M.-M.; Lu, H.-Y.; Zhang, P. Superconductivity of monolayer functionalized biphenylene with Dirac cones. *Phys. Chem. Chem. Phys.* **2023**, *25*, 2875.
(38) Veeravenkata, H. P.; Jain, A. Density functional theory driven phononic thermal conductivity prediction of biphenylene: A comparison with graphene. *Carbon* **2021**, *183*, 893.
(39) Zhang, P.; Ouyang, T.; Tang, C.; He, C.; Li, J.; Zhang, C.; Hu, M.; Zhong, J. The intrinsic thermal transport properties of the biphenylene network and the influence of hydrogenation: a first-principles study. *J. Mater. Chem. C* **2021**, *9*, 16945.
(40) Tong, Z.; Pecchia, A.; Yam, C.; Dumitrică, T.; Frauenheim, T. Ultrahigh electron thermal conductivity in T-graphene, biphenylene, and net-graphene. *Adv. Energy Mater.* **2022**, *12*, 2200657.
(41) Li, Q.; Zhou, J.; Liu, G.; Wan, X. Extraordinary negative thermal expansion of monolayer biphenylene. *Carbon* **2022**, *187*, 349.
(42) Xie, Z.-X.; Chen, X.-K.; Yu, X.; Deng, Y.-X.; Zhang, Y.; Zhou, W.-X.; Jia, P.-Z. Intrinsic thermoelectric properties in biphenylene nanoribbons and effect of lattice defects. *Comput. Mater. Sci.* **2023**, *220*, 112041.
(43) Yang, G.; Hu, Y.; Qiu, Z.; Li, B.-L.; Zhou, P.; Li, D.; Zhang, G. Abnormal strain-dependent thermal conductivity in biphenylene monolayer using machine learning interatomic potential. *Appl. Phys. Lett.* **2023**, *122*, 082202.
(44) Liu, T.; Jing, Y.; Li, Y. Two-dimensional biphenylene: A graphene allotrope with superior activity toward electrochemical oxygen reduction reaction. *J. Phys. Chem. Lett.* **2021**, *12*, 12230.
(45) Mane, P.; Kaur, S. P.; Chakraborty, B. Enhanced reversible hydrogen storage efficiency of zirconium-decorated biphenylene monolayer: A computational study. *Energy Storage* **2022**, *4*, e377.
(46) Asadi, L.; Saadati, Z.; Salehpour, M. Theoretical evaluation of Al-doped biphenylene nanosheet sensing properties toward gamma-butyrolactone. *Structural Chemistry* **2022**, *33*, 1947.
(47) Su, W.-S.; Yeh, C.-H. Theoretical investigation of methane oxidation reaction over a novel metal-free catalyst biphenylene network. *Diamond Relat. Mater.* **2022**, *124*, 108897.
(48) Al-Jayyousi, H. K.; Sajjad, M.; Liao, K.; Singh, N. Two-dimensional biphenylene: a promising anchoring material for lithium-sulfur batteries. *Sci. Rep.* **2022**, *12*, 4653.
(49) Han, T.; Liu, Y.; Lv, X.; Li, F. Biphenylene monolayer: a novel nonbenzenoid carbon allotrope with potential application as an anode material for high-performance sodium-ion batteries. *Phys. Chem. Chem. Phys.* **2022**, *24*, 10712.
(50) Chen, X.-W.; Lin, Z.-Z.; Li, X.-M. Biphenylene network as sodium ion battery anode material. *Phys. Chem. Chem. Phys.* **2023**, *25*, 4340.
(51) Niu, K.; Fan, Q.; Chi, L.; Rosen, J.; Gottfried, J. M.; Björk, J. Unveiling the formation mechanism of the biphenylene network. *Nanoscale Horiz.* **2023**, *8*, 368.
(52) Lv, F.; Liang, H.; Duan, Y. Funnel-shaped electronic structure and enhanced thermoelectric performance in ultralight $c_x(BN)_{1-x}$ biphenylene networks. *Phys. Rev. B* **2023**, *107*, 045422.
(53) Yang, N.; Yang, H.; Jin, G. Interface-induced topological phase and doping-modulated bandgap of two-dimensioanl graphene-like networks. *Chinese Physics B* **2023**, *32*, 017201.
(54) Armitage, N. P.; Mele, E. J.; Vishwanath, A. Weyl and Dirac semimetals in three-dimensional solids. *Rev. Mod. Phys.* **2018**, *90*, 015001.
(55) Wang, Y.; Liu, E.; Liu, H.; Pan, Y.; Zhang, L.; Zeng, J.; Fu, Y.; Wang, M.; Xu, K.; Huang, Z.; et al. Gate-tunable negative longitudinal magnetoresistance in the predicted type-II Weyl semimetal WTe2. *Nat. Commun.* **2016**, *7*, 13142.
(56) Chen, F.; Lv, H.; Luo, X.; Lu, W.; Pei, Q.; Lin, G.; Han, Y.; Zhu, X.; Song, W.; Sun, Y. Extremely large magnetoresistance in the type-II Weyl semimetal MoTe2. *Phys. Rev. B* **2016**, *94*, 235154.
(57) Kumar, N.; Sun, Y.; Xu, N.; Manna, K.; Yao, M.; Süss, V.; Leermakers, I.; Young, O.; Förster, T.; Schmidt, M.; et al. Extremely high magnetoresistance and conductivity in the type-II Weyl semimetals WP2 and MoP2. *Nat. Commun.* **2017**, *8*, 1642.
(58) Lai, J.; Liu, Y.; Ma, J.; Zhuo, X.; Peng, Y.; Lu, W.; Liu, Z.; Chen, J.; Sun, D. Broadband anisotropic photoresponse of the "hydrogen atom" version type-II Weyl semimetal candidate TaIrTe4. *ACS Nano* **2018**, *12*, 4055.
(59) Sadhukhan, K.; Politano, A.; Agarwal, A. Novel undamped gapless plasmon mode in a tilted type-II Dirac semimetal. *Phys. Rev. Lett.* **2020**, *124*, 046803.
(60) Togo, A. First-principles phonon calculations with phonopy and phono3py. *J. Phys. Soc. Jpn.* **2023**, *92*, 012001.
(61) Togo, A.; Chaput, L.; Tadano, T.; Tanaka, I. Implementation strategies in phonopy and phono3py. *J. Phys.: Condens. Matter* **2023**, *35*, 353001.
(62) Bergman, D. L.; Wu, C.; Balents, L. Band touching from real-space topology in frustrated hopping models. *Phys. Rev. B* **2008**, *78*, 125104.
(63) Leykam, D.; Andreanov, A.; Flach, S. Artificial flat band systems: from lattice models to experiments. *Advances in Physics: X* **2018**, *3*, 1473052.
(64) Rhim, J.-W.; Yang, B.-J. Classification of flat bands according to the band-crossing singularity of bloch wave functions. *Phys. Rev. B* **2019**, *99*, 045107.
(65) Ma, J.; Rhim, J.-W.; Tang, L.; Xia, S.; Wang, H.; Zheng, X.; Xia, S.; Song, D.; Hu, Y.; Li, Y.; et al. Direct observation of flatband loop states arising from nontrivial real-space topology. *Phys. Rev. Lett.* **2020**, *124*, 183901.
(66) Rhim, J.-W.; Yang, B.-J. Singular flat bands. *Advances in Physics: X* **2021**, *6*, 1901606.
(67) Hwang, Y.; Rhim, J.-W.; Yang, B.-J. Geometric characterization of anomalous landau levels of isolated flat bands. *Nat. Commun.* **2021**, *12*, 6433.
(68) Milićević, M.; Montambaux, G.; Ozawa, T.; Jamadi, O.; Real, B.; Sagnes, I.; Lemaître, A.; Le Gratiet, L.; Harouri, A.; Bloch, J.; et al. Type-iii and tilted dirac cones emerging from flat bands in photonic orbital graphene. *Physical Review X* **2019**, *9*, 031010.
(69) González-Herrero, H.; Gómez-Rodríguez, J. M.; Mallet, P.; Moaied, M.; Palacios, J. J.; Salgado, C.; Ugeda, M. M.; Veuillen, J.-Y.; Yndurain, F.; Brihuega, I. Atomic-scale control of graphene magnetism by using hydrogen atoms. *Science* **2016**, *352*, 437.
(70) Slot, M. R.; Gardenier, T. S.; Jacobse, P. H.; Van Miert, G. C.; Kempkes, S. N.; Zevenhuizen, S. J.; Smith, C. M.; Vanmaekelbergh, D.; Swart, I. Experimental realization and characterization of an electronic lieb lattice. *Nat. Phys.* **2017**, *13*, 672.

https://doi.org/10.1021/acs.nanolett.4c00314
Nano Lett. 2024, 24, 4885−4892

(71) Møller, M.; Jarvis, S. P.; Guérinet, L.; Sharp, P.; Woolley, R.; Rahe, P.; Moriarty, P. Automated extraction of single h atoms with stm: tip state dependency. *Nanotechnology* **2017**, *28*, 075302.
(72) Touhara, H.; Okino, F. Property control of carbon materials by fluorination. *Carbon* **2000**, *38*, 241.
(73) Padamata, S. K.; Yasinskiy, A.; Stopic, S.; Friedrich, B. Fluorination of two-dimensional graphene: A review. *J. Fluorine Chem.* **2022**, *255*−*256*, 109964.
(74) Wang, B.; Wang, J.; Zhu, J. Fluorination of graphene: A spectroscopic and microscopic study. *ACS Nano* **2014**, *8*, 1862.
(75) Chen, X.; Fan, K.; Liu, Y.; Li, Y.; Liu, X.; Feng, W.; Wang, X. Recent advances in fluorinated graphene from synthesis to applications: Critical review on functional chemistry and structure engineering. *Adv. Mater.* **2022**, *34*, 2101665.
(76) Feng, W.; Long, P.; Feng, Y.; Li, Y. Two-dimensional fluorinated graphene: Synthesis, structures, properties and applications. *Advanced Science* **2016**, *3*, 1500413.

https://doi.org/10.1021/acs.nanolett.4c00314
Nano Lett. 2024, 24, 4885−4892